Icarus 206 (2010) 83–94

Contents lists available at ScienceDirect

Icarus

journal homepage: www.elsevier.com/locate/icarus

# Large density fluctuations in the martian ionosphere as observed by the Mars Express radar sounder

D.A. Gurnett [a,*], D.D. Morgan [a], F. Duru [a], F. Akalin [a], J.D. Winningham [b], R.A. Frahm [b], E. Dubinin [c], S. Barabash [d]

[a] Department of Physics and Astronomy, University of Iowa, Iowa City, IA 52242, United States
[b] Southwest Research Institute, San Antonio, TX 78228-0510, United States
[c] Max-Planck-Institut, D-37191 Katlenburg-Lindau, Germany
[d] Swedish Institute of Space Physics, S-98128 Kiruna, Sweden

ARTICLE INFO

*Article history:*
Received 12 November 2008
Revised 20 January 2009
Accepted 25 February 2009
Available online 3 March 2009

*Keywords:*
Mars
Ionosphere

ABSTRACT

The MARSIS (Mars Advanced Radar for Subsurface and Ionosphere Sounding) instrument on the Mars Express spacecraft provides both local and remote measurements of electron densities and measurements of magnetic fields in the martian ionosphere. The density measurements show a persistent level of large fluctuations, sometimes as much as a factor of three or more at high altitudes. Large magnetic field fluctuations are also observed in the same region. The power spectrums of both the density and magnetic field fluctuations have slopes on a log–log plot that are consistent with the Kolmogorov spectrum for isotropic fluid turbulence. The fractional density fluctuation, $\Delta n_e/n_e$, of the turbulence increases with altitude, and reaches saturation, $\Delta n_e/n_e \sim 1$, at an altitude of about 400 km, near the nominal boundary between the ionosphere and the magnetosheath. The fluctuations are usually so large that a well-defined ionopause-like boundary between the ionosphere and the solar wind is seldom observed. Of mechanisms that could be generating this turbulence, we believe that the most likely are (1) solar wind pressure perturbations, (2) an instability in the magnetosheath plasma, such as the mirror-mode instability, or (3) the Kelvin–Helmholtz instability driven by velocity shear between the rapidly flowing magnetosheath and the ionosphere.



## 1. Introduction

The Mars Express spacecraft, which was placed in orbit around Mars on 25 December 2003 (Chicarro et al., 2004), carries a low-frequency radar called MARSIS (Mars Advanced Radar for Subsurface and Ionosphere Sounding) that is designed to perform subsurface and ionospheric soundings (Picardi et al., 2004). In this paper we present MARSIS observations of large density and magnetic field fluctuations in the martian ionosphere, mainly at high altitudes, above about 275 km. Prior to MARSIS the primary method of obtaining information about the martian ionosphere was from radio occultation measurements. This technique involves measuring the phase shift of the radio signal from a spacecraft as the spacecraft passes behind the planet. As the ray path passes through the ionosphere the plasma causes small deviations in the phase of the radio signal. With certain simplifying assumptions these phase deviations can be analyzed to give the vertical profile of the electron density in the region near closest approach of the ray path to the planet. The first radio occultation measurements at Mars were obtained from the Mariner 4 spacecraft, which flew by Mars in 1964 (Fjeldbo et al. 1966). Since then, radio occultation measurements of the martian ionosphere have been obtained from numerous spacecraft, including Mars 4, 5, and 6, Mariner 9, Vikings 1 and 2, Mars Global Surveyor, Mars Express, and Mars Reconnaissance Orbiter. For a discussion of the results from these and other spacecraft, see Savich and Samovol (1976), Zhang et al. (1990a,b), Luhmann and Brace (1991), Kliore (1992), Krymskii et al. (2003, 2004), Mendillo et al. (2004), and Pätzold et al. (2005).

The MARSIS ionospheric sounder nicely complements the radio occultation measurements by providing improved spatial resolution and the ability to make measurements in regions not accessible to radio occultation measurements. Together these two techniques have now provided a good description of the main features of the martian ionosphere, including its interaction with the solar wind and the influence of crustal magnetic fields (Gurnett et al. 2005; Duru et al. 2006; Nielsen et al. 2006, 2007; Gurnett et al. 2008; Morgan et al. 2008). One area that has not yet been adequately explored is the occurrence of large density fluctuations at high altitudes, above about 300 km, in the region where the solar wind interacts with the ionosphere. At Venus large amplitude magnetic field fluctuations are generated in the magnetosheath

* Corresponding author.
*E-mail address:* donald-gurnett@uiowa.edu (D.A. Gurnett).

0019-1035/$ - see front matter © 2009 Elsevier Inc. All rights reserved.
doi:10.1016/j.icarus.2009.02.019

downstream of the shock by the mirror-mode instability (Volwerk et al., 2008). The velocity shear between the solar wind and the ionosphere is also known to cause large density fluctuations and turbulent mixing via the Kelvin–Helmholtz instability (Terada et al. 2002, 2004). The momentum transfer associated with the Kelvin–Helmholtz instability is believed to play a key role in the transport and loss of ions from the ionosphere. Similar turbulent transport effects driven by the Kelvin–Helmholtz instability have been predicted to occur at Mars (Penz et al. 2004). That such processes may be occurring in the upper ionosphere of Mars is supported by radio occultation measurements that show the presence of large density fluctuations from about 150 to 200 km, near the upper altitude limit of the radio occultation technique (Wang and Nielsen 2002, 2003). Recent local electron density measurements from MARSIS have shown that similar large density fluctuations are present at even higher altitudes, from about 250 to 800 km (Duru et al. 2008), in the region where the Kelvin–Helmholtz and mirror-mode instabilities are expected to occur. The purpose of this paper is to further investigate these large density fluctuations using both local and remote electron density measurements from MARSIS.

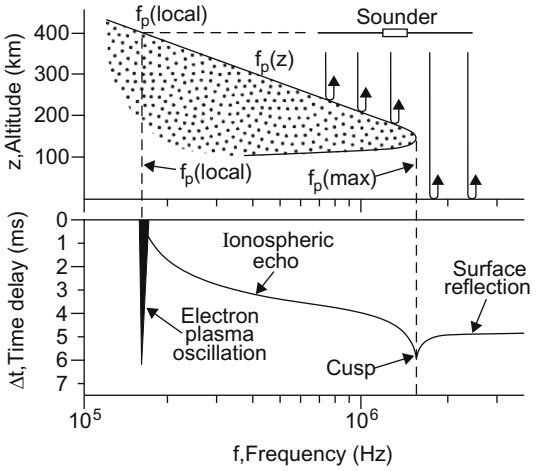


**Fig. 1.** The top panel shows a representative profile of the electron plasma frequency, $f_p$, as a function of altitude, $z$, in the martian ionosphere. The bottom panel shows a plot of the time delay, $\Delta t$, for a radar pulse at a frequency, $f$, to reflect and return to the spacecraft. The intense vertical spike labeled "electron plasma oscillation" is caused by the excitation of electrostatic electron plasma oscillations at the local electron plasma frequency, $f_p$(local). The cusp in the ionospheric echo occurs at the maximum plasma frequency in the ionosphere, $f_p$(max). This cusp separates the ionospheric echo from the surface reflection.

## 2. Ionospheric radar sounding techniques and limitations

To understand the techniques and limitations of MARSIS for measuring ionospheric density fluctuations it is useful to give a brief discussion of the operation of the instrument and the interpretation of the data. MARSIS consists of a 40-m tip-to-tip electric dipole antenna, a transmitter, a receiver, and a digital data processing system (Picardi et al. 2004). In the ionospheric sounding mode, the MARSIS transmitter is sequentially stepped through 160 quasi-logarithmically spaced frequencies ($\Delta f/f \sim 2\%$) from 0.1 to 5.4 MHz. At each step a 91.4 μs quasi-sinusoidal pulse is transmitted at a fixed frequency, $f$, and the intensities of the resulting ionospheric echoes are recorded as a function of delay time, $\Delta t$, in 80 equally space time bins from 0 to 7.31 ms. A complete scan of all 160 frequencies takes 1.26 s, and the basic sweep cycle is repeated once every 7.54 s. The acquisition of MARSIS data is strongly controlled by the spacecraft orbit. Mars Express is in a highly eccentric orbit with a periapsis altitude of about 275 km, an apoapsis altitude of about 11,000 km, and a period of 6.75 hr (Chicarro et al. 2004). Because of signal-to-noise limitations, ionospheric sounding data is only collected when the spacecraft is near periapsis, where the range to the ionosphere is relatively small, about a thousand km, or less. A typical ionospheric sounding pass starts on the inbound leg at an altitude of about 1200 km, continues through periapsis at about 275 km, and ends on the outbound leg at an altitude of about 1200 km. The total duration of an ionospheric sounding pass is usually about 40 min.

The interpretation of the ionospheric sounder data is illustrated in Fig. 1. The top panel shows a typical profile of the electron plasma frequency, $f_p(z)$, in the ionosphere as a function of altitude, $z$. The electron plasma frequency is determined by the electron density, which is given by $f_p = 8980\ \sqrt{n_e}$ Hz, where the electron number density, $n_e$, is in $cm^{-3}$ (Gurnett and Bhattacharjee, 2005). Two types of electron density measurements can be made, remote and local. The remote measurements rely on the reflection of the transmitted radio wave by the ionosphere. Radio waves cannot propagate at frequencies below the electron plasma frequency, which is the region indicated by the shading in Fig. 1. For vertical incidence on a horizontally stratified ionosphere, the radio wave emitted by the transmitter is reflected at the altitude where the wave frequency is equal to the electron plasma frequency, $f = f_p$. By sequentially advancing the frequency of the transmitter after each pulse, the time delay, $\Delta t(f)$, of the resulting echo can be measured as a function of frequency. The received echo intensities are usually displayed on a two-dimensional plot of time delay and frequency, as shown by the sketch in the bottom panel of Fig. 1. This type of plot is called an ionogram (Gurnett et al. 2005). As the frequency increases from the left-hand side of the ionogram, ionospheric echoes first occur (at zero time delay) when the frequency reaches the local plasma frequency, $f_p$(local). As the frequency increases further, the time delay gradually increases as the range to the reflection point increases. A rough estimate of the range to the reflection point is given by $(1/2)c\Delta t$, where $c$ is the speed of light. This distance is called the apparent range. The factor of one-half is included because $\Delta t$ is the round-trip time delay. For accurate measurements the effect of the plasma on the propagation speed must be considered. This effect is called dispersion. From basic principals of wave propagation (Gurnett and Bhattacharjee, 2005) it can be shown that the propagation speed of the pulse is given by

$$(v_g = c\sqrt{1 - (f_p/f)^2},$$

where $v_g$ is the group velocity. From this equation it is easy to show that the round-trip time delay is given by

$$\Delta t(f) = \frac{2}{c}\int_{z(f_p)}^{z_{sc}} \frac{dz}{\sqrt{1 - (f_p(z)/f)^2}}, \qquad (1)$$

where the integration is carried out from the altitude of the reflection point, $z(f_p)$, to the altitude of the spacecraft, $z_{sc}$. At the maximum plasma frequency in the ionosphere, $f_p$(max), a "cusp" forms in the echo trace, as shown in Fig. 1. The cusp occurs because the group velocity of the pulse goes to zero over an increasingly long path length as the frequency approaches the peak in the plasma frequency profile. As soon as the transmitter frequency exceeds $f_p$(max) the pulse passes through the ionosphere, where it subsequently reflects from the surface of the planet and returns to the spacecraft. The resulting echo is labeled "surface reflection" in Fig. 1.

To compute the electron density profile from the measured time delay, $\Delta t(f)$, the integral in Eq. (1) must be inverted to give $z(f_p)$, the altitude of the reflection point as a function of plasma frequency. The solution of this integral equation, called Abel's equation, is a

classical problem in mathematics (Whittaker and Watson, 1927), and has a formal solution (Budden, 1961) given by

$$z(f_p) = \frac{1}{\pi}\int_{\alpha_0}^{\pi/2} c\Delta t(f_p \sin\alpha)d\alpha, \quad (2)$$

where $\sin\alpha_0 = f_p(z_{sc})/f_p$. Because the radiated power from the dipole antenna decreases rapidly at low frequencies, time delay measurements often do not extend down to the local plasma frequency, $f_p$(local). In such cases, the time delay must be interpolated between the local plasma frequency at the spacecraft, $f_p$(local), and the lowest frequency for which an echo can be detected. For a discussion of the techniques used to do this interpolation, and the errors introduced, see Morgan et al. (2008).

Although remote echoes often do not extend down to the local electron plasma frequency, it is still usually possible to determine the electron plasma frequency. As the transmitter frequency passes through the local electron plasma frequency, strong local electrostatic oscillations are excited in the plasma. These oscillations are called electron plasma oscillations or Langmuir waves (Gurnett and Bhattacharjee, 2005), and produce the intense vertical spike labeled "electron plasma oscillation" in the ionogram at the bottom of Fig. 1. This signal is so strong that even when the electron plasma frequency is below the 0.1 MHz low frequency limit of the receiver, the local plasma frequency can usually be determined from harmonics generated by nonlinear distortion in the receiver. The high order of these harmonics greatly improves the accuracy to which the fundamental oscillation frequency can be measured. Usually the oscillation frequency can be measured to an accuracy of about 1–2% which, if there are no other sources of error, translates to an overall accuracy for the electron density measurement of about 2–4%.

Thermal effects can produce errors in the density measurements by causing an upward shift of the oscillation frequency relative to the plasma frequency. However, in the martian ionosphere this error is normally very small. It is relatively easy to show that the fractional shift in the oscillation frequency is given by $\Delta\omega/\omega = (3/2)k^2\lambda_D^2$, where $k = 2\pi/\lambda$ is the wave number, $\lambda$ is the wavelength, $\lambda_D = 6.9\sqrt{T_e/n_e}$ is the Debye length in cm, $T_e$ is the electron temperature in K, and $n_e$ is the electron density in $cm^{-3}$ (Gurnett and Bhattacharjee, 2005). This frequency shift is usually negligible because the Debye length is normally much smaller than the wavelength, $\lambda \sim 40$ m, of the electrostatic waves excited by the antenna. For the parameters that exist in the martian ionosphere ($n_e \sim 10^4$–$10^5$ $cm^{-3}$, $T_e \sim 2000$ K) the Debye length is only a few tens of centimeters, see Duru et al. (2008). Thermal corrections can be important in the solar wind, where the plasma is more tenuous ($n_e \sim 3$ $cm^{-3}$) and hotter ($T_e \sim 10^5$ K). However, in the solar wind the electron plasma oscillations usually cannot be detected because the wave packet is rapidly carried away from the spacecraft by the high flow velocity. The threshold flow velocity, above which plasma oscillations cannot be detected, is estimated by Duru et al. (2008) to be about 160 km/s.

Although Mars Express does not have a magnetometer, it turns out that the local magnetic field strength can also be measured by MARSIS. The technique used is based on the discovery that a burst of electrons is accelerated by the high voltage, ~500 V, imposed on the antenna during each cycle of the transmitter waveform (Gurnett et al., 2005, 2008). Once accelerated, the electrons orbit in the local magnetic field and produce a series of voltage pulses on the antenna. The repetition rate of the pulses is the electron cyclotron frequency, $\omega_c = (e/m)B$, where $e/m$ is the charge-to-mass ratio of the electron, and $B$ is the magnetic field strength. A sketch of the pulses as they appear on an ionogram is shown in Fig. 2, along with the resulting cyclotron motion of the accelerated electrons. These pulses are called "electron cyclotron echoes." By measuring the

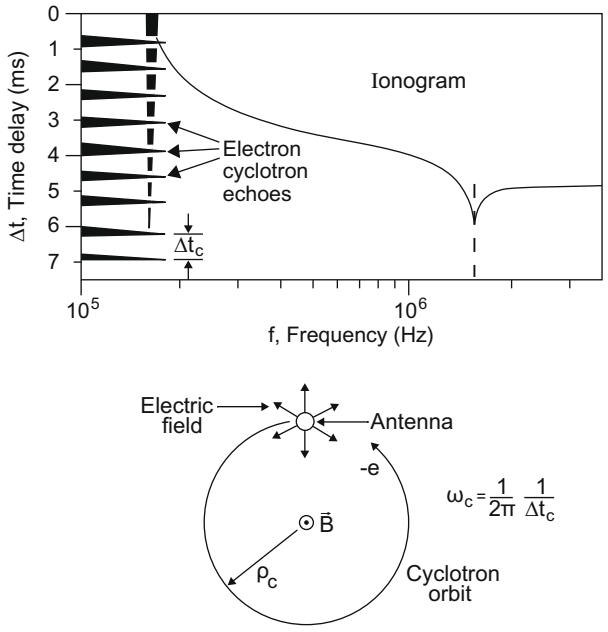


**Fig. 2.** The electron cyclotron echoes appear as a series of horizontal equally spaced spikes in the plot of time delay, $\Delta t$, as a function of frequency, $f$, as shown in the top panel. The echoes are produced by ambient electrons that are accelerated in the vicinity of the antenna by the large electric fields during the transmit pulse. As shown in the bottom diagram, these electrons then orbit in the magnetic field, **B**, and produce a voltage pulse on the antenna every time they return to the vicinity of the antenna.

period, $\Delta t_c$, of the cyclotron echoes the magnetic field strength can be determined using the equation $B = 2\pi(m/e)(1/\Delta t_c)$. Since the echoes are repeated many times, the magnetic field strength can usually be measured with very good accuracy, typically a few percent or less. The region over which the magnetic field is sampled is controlled by the radius of the cyclotron orbit, $\rho_c$, which depends on the magnetic field strength. For a typical antenna voltage of 500 V and a magnetic field strength of 100 nT, the radius of the cyclotron orbit is about $\rho_c \sim 1$ km.

## 3. Local density measurements

Since our main focus is on high altitudes where the solar wind interaction with the ionosphere is expected to occur, we start by discussing the local electron densities derived from the excitation of electron plasma oscillations. The electron plasma oscillation technique provides electron density measurements at much higher altitudes than can be obtained from remote soundings. The data set used for the local density measurements is from Duru et al. (2008) and consists of 503 periapsis passes from August 4, 2005, to July 31, 2007. To illustrate the type of density fluctuations observed in these data, the top panels of Figs. 3 and 4 show the densities (black lines) obtained during two dayside periapsis passes, on orbits 2198 and 3231. The bottom panels show the corresponding electron energy spectrums obtained from the ASPERA electron spectrometer (ELS). For a description of the ASPERA-ELS instrument, see Barabash et al. (2004). As can be seen, very large electron density fluctuations are present during both passes, particularly on orbit 2198. The amplitudes of the fluctuations vary from as small as a few percent, which is near the resolution of the measurements, to very large values, sometimes as much as a factor of five.

Sometimes isolated well-defined steps occur in the electron densities that stand out above the general background of fluctuations. Examples of such steps occur at about 04:36 and 04:50 Uni-

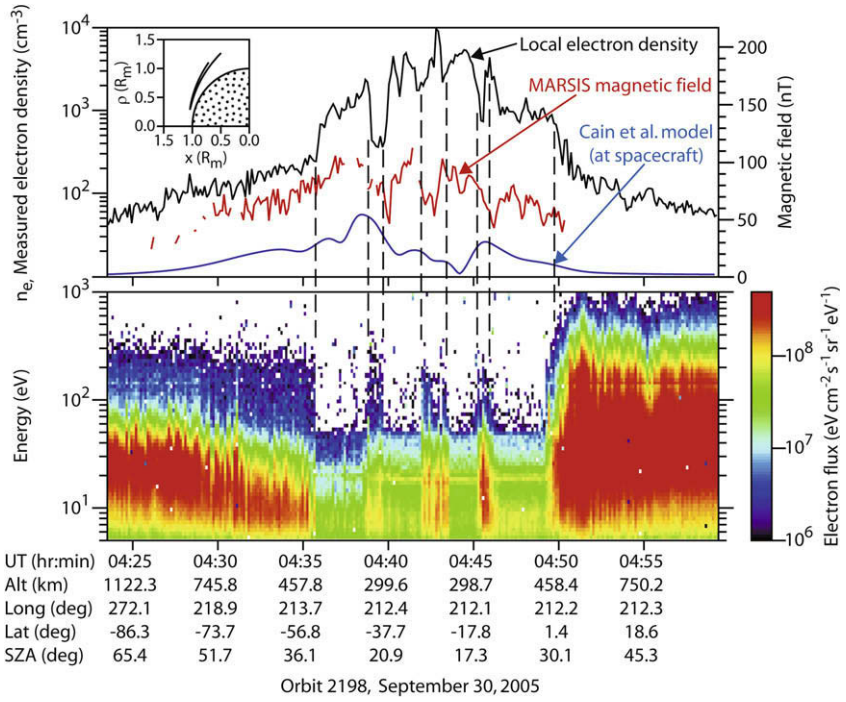


**Fig. 3.** The black line in the top panel shows the local electron density obtained from the frequency of locally excited electron plasma oscillations during a typical dayside pass through the martian ionosphere. The red line shows the local magnetic field strength determined from electron cyclotron echoes (see Gurnett et al. 2005), and the blue line shows the crustal magnetic field strength at the spacecraft computed from the model of Cain et al. (2003). The bottom panel shows the corresponding color-coded electron intensity spectrums from the ASPERA-ELS spectrometer. The Universal Time (UT), altitude (Alt), longitude (Long), latitude (Lat) and solar zenith angle (SZA) of the spacecraft are shown at the bottom of the plot. Periapsis is near the center of the plot. The little box at the upper left shows the spacecraft trajectory in a coordinate system in which the $x$ axis is along a line from the center of the planet to the Sun, and $\rho$ is the perpendicular distance from this line. The inbound and outbound trajectories are almost identical in this coordinate system. Note that the decreases in the electron density near periapsis are closely correlated with increases in the electron intensities, indicating solar wind incursions deep into the ionosphere.

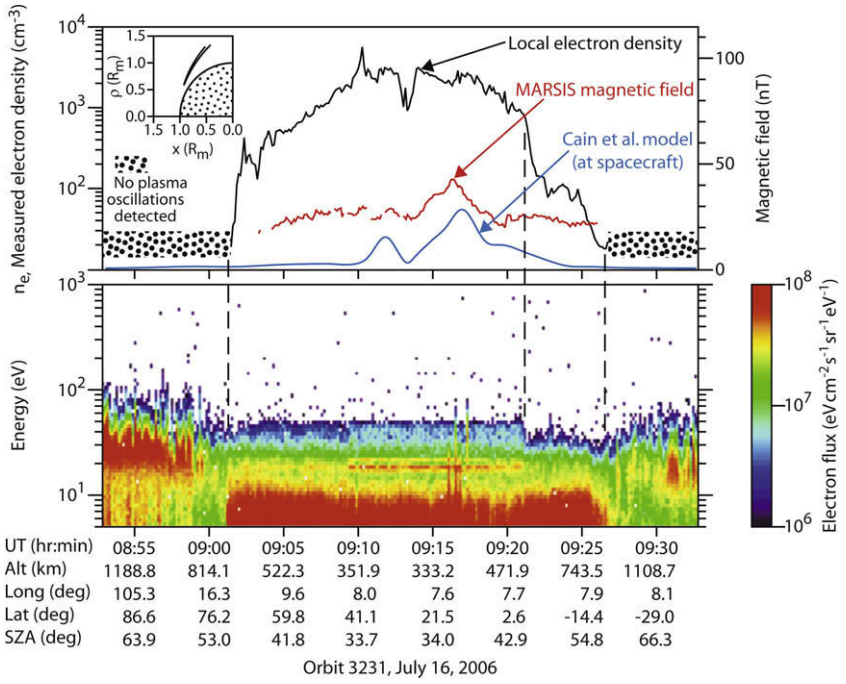


**Fig. 4.** The local electron density, magnetic field strength and low-energy electron intensities for another dayside pass similar to Fig. 3, but about one year later. Again a persistent level of density and magnetic field fluctuations is observed during the entire pass, very similar to Fig. 3, but of somewhat lower amplitudes. No electron plasma oscillations were observed before 09:01 UT and after 09:27 UT, most likely because the spacecraft was in the solar wind where they are carried away from the spacecraft before they can be detected.

versal Time (UT) in Fig. 3, and again at about 09:01 UT in Fig. 4. These density steps are reminiscent of the abrupt density steps that occur at the ionopause at Venus (Brace et al. 1983), which is the boundary between the magnetosheath and the ionosphere. On the dayside of Mars the ionopause is expected to occur at an altitude of approximately 400 km (Trotignon et al. 2006; Dubinin et al. 2006). The ELS spectrums in bottom panels of Figs. 3 and 4 generally do not show comparable density steps, because the ELS instrument is not able to detect the cold ionospheric component of the plasma. The variations that do occur in the ELS spectrums tend to occur at the upper altitude limit of the relatively cold ionospheric plasma. The magnetosheath plasma, which is indicated by the intense (red) electron energy spectrums from about $10^1$–$10^2$ eV, typically does not penetrate inside of the ionopause-like density steps. Typically, the transition on the magnetosheath side is not nearly as sharp and well defined as on the ionosphere side. Note the upward ramp in the electron density and the corresponding decrease in the electron energy before the abrupt step in the density at 04:36 UT in Fig. 3, and the depression in the low energy electron intensities in the 3 min interval just before the abrupt density step at 09:01 UT in Fig. 4. These features indicate that there is considerable mixing of the solar wind and ionospheric plasmas in the region immediately outside of these "ionopause-like" density steps.

Although ionopause crossings are usually very well defined at Venus, such well-defined "ionopause" crossings seldom occur at Mars. For example, although the inbound pass in Fig. 4 has a very sharp "ionopause-like" density step at 09:01 UT, the outbound pass, which occurs at almost the same altitudes (Alt) and solar zenith angles (SZA), does not have a similar density step. After surveying a large number of passes, our impression is that large well-defined "ionopause" crossings, similar to those that occur at Venus, are rare in the MARSIS data. In contrast, the electron densities in the region near and below the nominal ionopause altitude are usually characterized by very large fluctuations. These fluctuations are clearly evident in the top panels of both Figs. 3 and 4. The density fluctuations are especially large in Fig. 3 and consist of many irregular density jumps, marked by the vertical dashed lines. These density jumps are seen to be closely correlated with corresponding out-of phase jumps in the ELS electron intensities. The general trend is for the ELS electron intensities to decrease when the local electron density increases, indicating encounters with the magnetosheath plasma. These variations show that the density fluctuations are closely correlated with irregular motions of the magnetosheath boundary, causing what appear to be transient incursions of the magnetosheath plasma into the ionosphere, often down to very low altitude, sometimes well below 300 km.

It is interesting to investigate whether the local density fluctuations described above have corresponding magnetic field fluctuations. The red lines in the top panels of Figs. 3 and 4 show the magnetic field strengths determined using the electron cyclotron echo technique. For comparison, the blue lines show the crustal magnetic field strengths (Acuña et al. 1998, 1999; Connerney et al. 2005) computed at the spacecraft from the multipole magnetic field model of Cain et al. (2003). As can be seen, the local magnetic field measurements generally follow the Cain et al. model with an offset of about 50 nT for orbit 2198, and about 15 nT for orbit 3231. These offsets are believed to be due to solar wind induced currents that flow at high altitudes in the dayside ionosphere. For a further discussion of these induced currents see Brain et al. (2003, 2006). The magnetic field of these induced currents are not included in the Cain et al. model, which is based on low altitude nightside measurements where the crustal magnetic fields are the dominant component.

As with the local electron density, the local magnetic field also has large fluctuations. Similar magnetic fluctuations have been previously reported by Brain (2007) in the magnetic field data from Mars Global Surveyor (MGS). Although it sometimes appears that the magnetic field fluctuations may have some relation to spatial variations in the underlying crustal magnetic field, as in Fig. 3, the density and magnetic field fluctuations are commonly observed over the northern hemisphere, which has almost no crustal magnetic fields. Therefore, although crustal magnetic fields may play some role in certain cases, the persistent level of large density and magnetic field fluctuations commonly observed on the dayside of Mars cannot be solely attributed to crustal magnetic fields. Often the amplitude of the magnetic field fluctuations is larger when the density fluctuations are larger (compare Figs. 3 and 4), suggesting that both have a common cause. Possible explanations are that the fluctuations are propagating as a magnetohydrodynamic (MHD) wave, such as the compressional Alfvén wave, or as non-propagating mirror-mode wave (Tsurutani et al. 1982; Volwerk et al., 2008), both of which have density and magnetic field fluctuations. Although the waveforms of the density and magnetic field sometimes show a detailed one-to-one correspondence, usually the correlation between the two waveforms is poor. This suggests that the fluctuations have a significant shear component, such as the shear Alfvén wave, which has no density fluctuations. Unfortunately, because the electron cyclotron echo technique does not give the magnetic field direction, our ability to analyze these fluctuations in terms of various possible MHD modes is quite limited. It is also possible that more complicated magnetic field structures might be involved, such as flux ropes, which are commonly observed in the ionospheres of both Venus and Mars (Russell and Elphic, 1979; Vignes et al., 2004).

Since the electron density and magnetic field fluctuations appear to have a significant turbulent component, it is of interest to compute the power spectrums of these fluctuations and compare them with the expectations of fluid turbulence theory. Power spec-

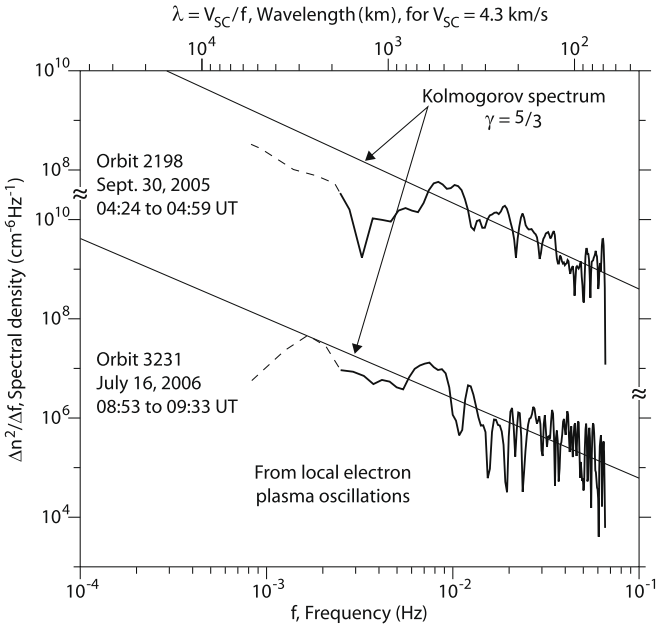


**Fig. 5.** The power spectrum, $\Delta n_e^2/\Delta f$, of the local electron density fluctuations observed during orbits 2198 and 3231 in Figs. 3 and 4 plotted as a function of frequency, $f$, on a log–log plot. The scale at the top shows the corresponding wavelength, $\lambda = V_{sc}/f$, assuming that the spacecraft is moving through a completely static density structure. The straight lines show the Kolmogorov ($\gamma = 5/3$) inverse power-law spectrum expected for isotropic three-dimensional turbulence. At the longest wavelengths (shown by the dashed lines) the spectrums are contaminated to some extent by the spatial variations induced by the changing altitude of the spacecraft. Nevertheless, the spectrums are in reasonably good agreement with the Kolmogorov spectrum.

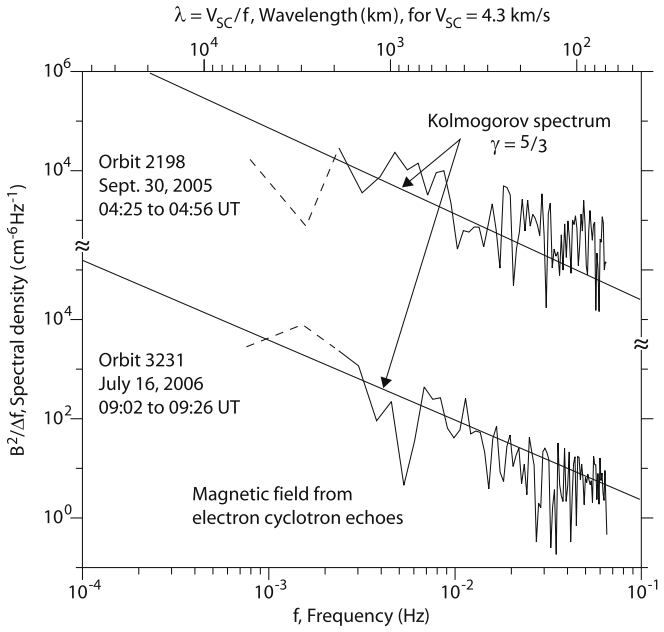


**Fig. 6.** The power spectrum, $B^2/\Delta f$, of the local magnetic field fluctuations observed during orbits 2198 and 3231 in Figs. 3 and 4 plotted as a function of frequency, $f$, on a log–log plot similar to Fig. 5. The magnetic field measurements were obtained from MARSIS using the electron echo technique. Again, at the longest wavelengths (shown by the dashed lines) the spectrums are contaminated to some extent by the spatial variations induced by the changing altitude of the spacecraft. However, as in Fig. 5 the power spectrums are reasonably consistent with the Kolmogorov spectrum.

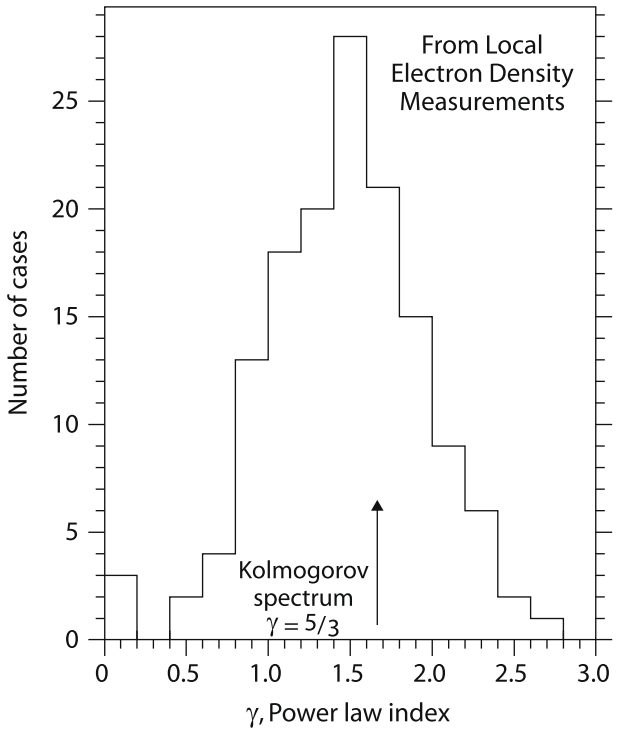


**Fig. 7.** A histogram of the index, $\gamma$, for the best-fit of the inverse power law $(1/f)^{\gamma}$ to the local electron density fluctuations observed on 142 passes through the dayside ionosphere of Mars. Although there is some scatter, the mean ($\gamma = 1.46$) and the peak ($\gamma = 1.55$) of the distribution are consistent with the Kolmogorov ($\gamma = 5/3$) spectrum.

trums of the electron density fluctuations in Figs. 3 and 4 are shown in Fig. 5. Although the power spectrums, $\Delta n_e^2/\delta f$, are plotted as a function of frequency, $f$, because of the high spacecraft velocity relative to the ionosphere it is reasonable to assume that the fluctuations are primarily due to the spacecraft motion through essentially static structures. To characterize the scale size of these structures, at the top of the plot we show the corresponding wavelength, $\lambda = V_{sc}/f$, computed using a spacecraft velocity of $V_{sc} = 4.3$ km/s, which is a typical horizontal velocity near periapsis. Although the density measurements on the two passes were obtained almost a year apart the spectrums are remarkably similar. Both spectrums decrease approximately as straight lines on this log–log plot, which indicates a power-law relationship. Although the long wavelength component of the spectrums (indicated by the dashed lines) are affected somewhat by the vertical component of the spacecraft motion through the ionosphere, the spectrums are nevertheless remarkably close to the $(1/f)^{5/3}$ Kolmogorov spectrum expected for isotropic three-dimensional fluid turbulence (Kolmogorov, 1941). Power spectrums of the magnetic field fluctuations, $B^2/\Delta f$, observed during these same two passes are shown in Fig. 6. The magnetic field spectrums also show a close similarity to the Kolmogorov spectrum.

To determine if the spectrums of the local density fluctuations are generally consistent with the Kolmogorov spectrum, we have computed the best root-mean-square fit of an inverse power law, $(1/f)^{\gamma}$, to the density spectrums for 142 passes through the dayside ionosphere. A histogram of the resulting power law indices is shown in Fig. 7. Although there is some spread in the distribution, the average, $\langle\gamma\rangle = 1.45$, and the peak, $\gamma_{peak} = 1.55$, of the distribution are reasonably consistent with the $\gamma = 5/3$ Kolmogorov spectrum.

## 4. Comparison to remote soundings

Since the local electron density measurements described above are limited to altitudes above about 275 km, it is of interest to determine whether comparable electron density fluctuations are observed in the remote sounding measurements, which are for much lower altitudes, generally below 275 km. For the remote sounding measurements we use the data from Morgan et al. (2008), which consists of ionograms from 375 periapsis passes. This data set consists of electron density profiles expressed as altitudes $z(n_{ei})$ as a function of the electron density, $n_{ei}$, one for each of the fixed sounding frequencies, $f_i$. The time resolution of these measurements is 7.54 s, which yields approximately 300 density profiles during a given pass. In order to generate a time series comparable to the local electron densities, we have interpolated the electron density profiles to a series of fixed altitudes, and then plotted the electron density as a function of time at these altitudes. Examples of such remote sounding measurements are shown in Figs. 8 and 9, which are for the same passes shown earlier in Figs. 3 and 4. The top panel in each figure gives the local electron density at the spacecraft, and the next three panels give the electron densities from the remote sounding measurements at altitudes of 220 km, 200 km, and 180 km. The second panel from the bottom shows the peak density in the ionosphere (black line) and the altitude of the peak density (red line), and the bottom panel shows the surface elevation (red line) directly below the spacecraft and the Cain et al. (2003) magnetic field model (black line) evaluated at an altitude of 250 km.

As can be seen from Figs. 8 and 9, the electron densities from the remote soundings show considerable fluctuations at all altitudes, especially for orbit 2198, which has a generally higher level of both local and remote density fluctuations than for orbit 3231. Comparisons of the plots at altitudes of 180, 200, and 220 km show that the density fluctuations are well correlated between adjacent altitudes. However, comparisons to the local density measurements do not show a good one-to-one correlation. The poor correlation between the local and remote measurements is most likely

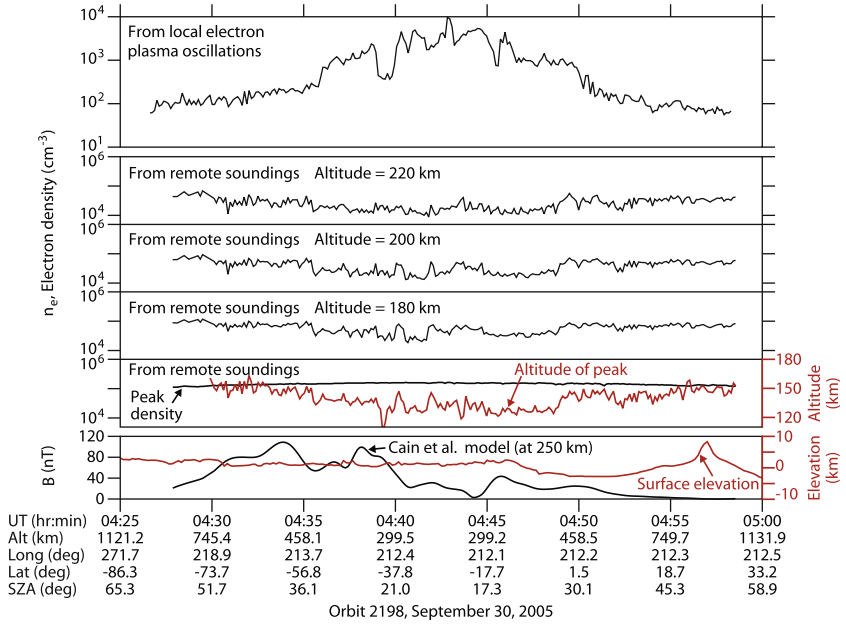


**Fig. 8.** A comparison of the local electron density fluctuations during orbit 2198 in Fig. 3 with the electron densities obtained from remote soundings taken during the same pass. The top panel shows the local electron density obtained from electron plasma oscillations; the next three panels show the electron densities obtained from remote soundings at altitudes of 220 km, 200 km, and 180 km, respectively; the next panel shows the peak density in the ionosphere (black line) and the altitude of the peak density (red line); and the bottom panel shows the elevation (red line) of the surface of Mars computed using the Mars Global Surveyor MOLA surface elevation model and the crustal magnetic strength (black line) computed at an altitude of 250 km from the Cain et al. (2003) magnetic field model. The density fluctuations from the remote soundings generally show a good one-to-one correlation for altitude separations on the order of 20 km. However, the correlation decreases with increasing altitude separation beyond about 20 km. The correlation decreases to the point that no correlation is evident with the local density measurements, which are generally separated from the remote measurements by altitudes of 100 km or more. The density fluctuations show no obvious correlation with variations in either the surface elevation or the crustal magnetic field strength.

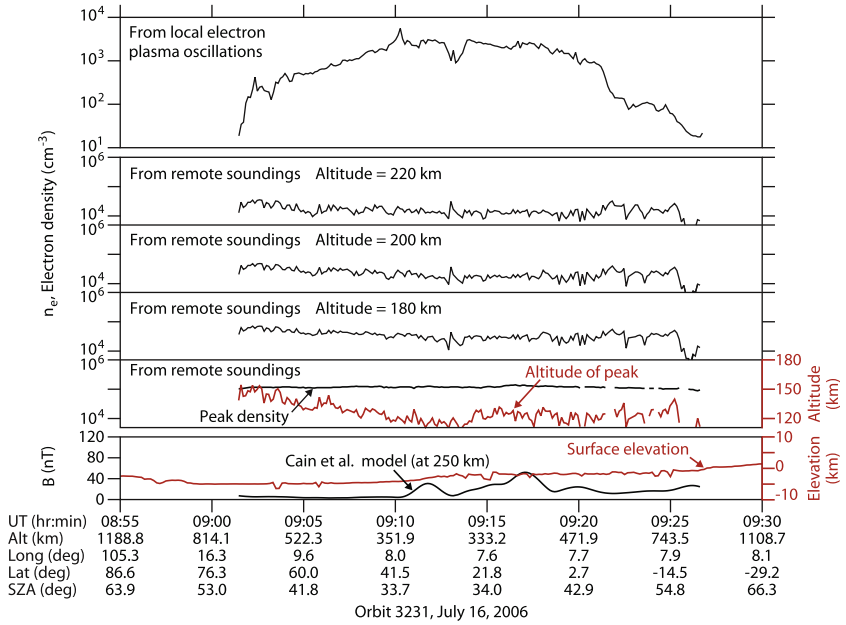


**Fig. 9.** A comparison, similar to Fig. 8, of the local electron density fluctuations during orbit 3231 in Fig. 4 with fluctuations in the electron density obtained from remote soundings taken during the same pass. Large electron density fluctuations can be seen in both the local and remote measurements, but not as large as in Fig. 8. Again, the density fluctuations from the remote soundings generally show a good one-to-one correlation between adjacent altitudes, but a poor correlation with the local density measurements at much higher altitudes. The density fluctuations show no obvious correlation with either the surface elevation or the crustal magnetic field strength.

due to the considerably larger altitude separation between these measurements, which is generally 100 km, or more. Even in the remote sounding data it is evident that the correlation decreases as the altitude separation increases (compare the fluctuations at 180 km with the fluctuations at 200 and 220 km). Note also that the peak electron density in the ionosphere is almost completely smooth, with no evidence of fluctuations comparable to those present at 180 km. Nevertheless, there are significant fluctuations in the altitude of the peak that are generally well correlated with the density fluctuations at 180 km. This suggests that the density

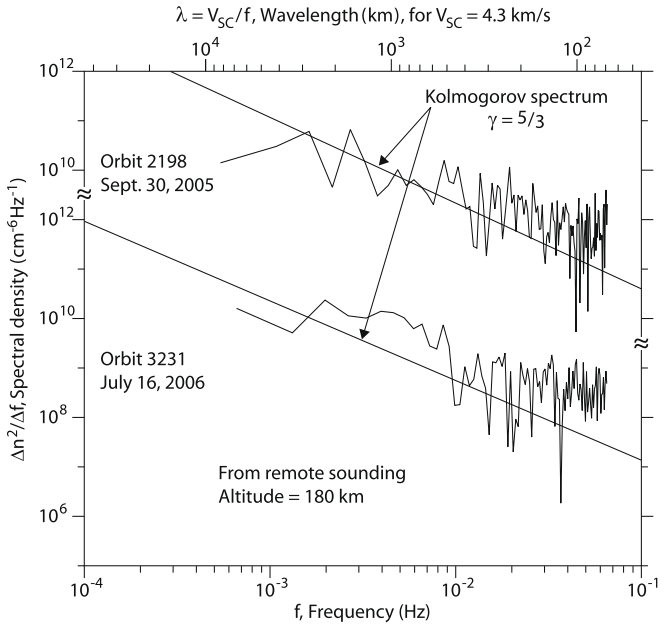


**Fig. 10.** The power spectrums, $\Delta n_e^2/\Delta f$, of the electron density fluctuations at an altitude of 180 km in Figs. 8 and 9 plotted as a function of frequency, $f$. The corresponding wavelength, $\lambda = V_{SC}/f$, is shown at the top of the plot, assuming that the sounder is sampling a time-stationary distribution of spatial fluctuations at a horizontal spacecraft velocity of $V_{SC}$ = 4.3 km/s. Both spectrums agree well with the Kolmogorov spectrum at low frequencies and long wavelengths, but tend to flatten somewhat at high frequencies and short wavelengths. The flattening of the spectrum at high frequencies is believed to be due to small random range errors introduced by the quantization of the time delay measurements. These errors introduce a flat background in the spectrum, below which the real density fluctuations cannot be detected.

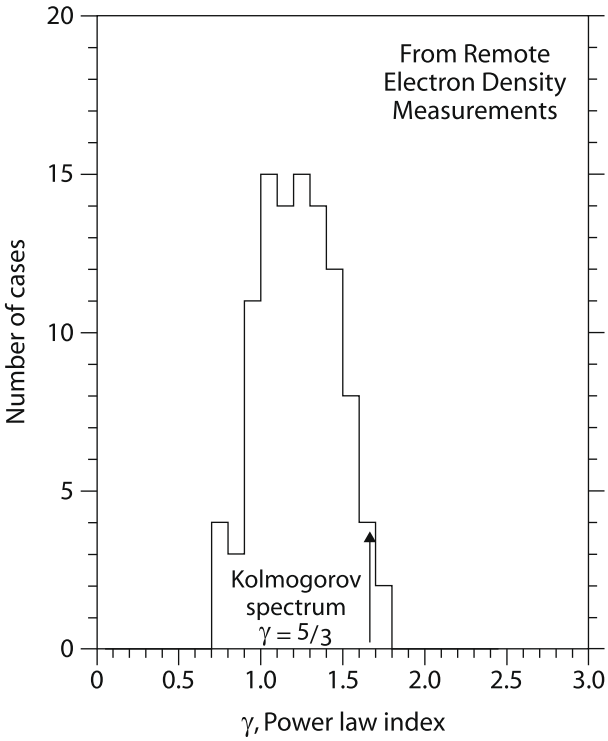


**Fig. 11.** A histogram of the power-law index (comparable to Fig. 7) for the best-fit inverse power law $(1/f)^{\gamma}$ to the electron density fluctuation spectrums obtained from 102 remote sounding passes interpolated to an altitude of 180 km The shift toward values less than the Kolmogorov index is probably caused by quantizing noise which tends to flatten the spectrum at high frequencies.

fluctuations near the peak in the ionosphere consist mainly of vertical motions with amplitudes ranging from 5 km to sometimes as large as 10 to 20 km.

Radio occultation measurements have previously shown that large density fluctuations are present in the lower levels of the ionosphere. Some of these fluctuations are known to be related to surface topography (Wang and Nielsen 2004), and others are known to be associated with variations in the crustal magnetic field (Krymskii et al. 2004; Withers and Mendillo, 2005). Although the bottom panels of Figs. 8 and 9 show that there are significant variations in both the surface elevation and the crustal magnetic field during both of these passes, no obvious one-to-one correlation is evident between these variations and the fluctuations in the ionospheric density. Although oblique echoes from isolated small-scale ionospheric structures have been associated with regions where the crustal magnetic field is vertical (Gurnett et al. 2005; Duru et al. 2006; Nielsen et al. 2006), the persistent overall level of density fluctuations observed in nearly all of the remote sounding data shows no relationship to the presence or absence of crustal magnetic fields immediately below the spacecraft.

Since the local and remote density measurements are obtained at quite different altitudes, it is interesting to compare the power spectrums of density fluctuations in the remote measurements with the power spectrums of the local density measurements. Fig. 10 shows the power spectrums of the remote electron density measurements at an altitude of 180 km for the two passes in Figs. 8 and 9. As with the local density spectrums in Fig. 5, the power spectrums both have slopes on the log–log plot that are in reasonable agreement with the Kolmogorov spectrum. However, the agreement is not as good as for the power spectrum of the local measurements in Fig. 5. In particular, the spectrum from the remote measurements tends to flatten somewhat at high frequencies and short wavelengths. This flattening of the spectrum is somewhat more noticeable for orbit 3231, which has a lower level of density fluctuations, than for orbit 2198. The flattening of the spectrum at high frequencies is believed to be due to quantization of the time delay measurements. This quantization sets a root-mean-square floor on the range resolution of about 5 km, and introduces a flat background noise level below which real density fluctuations cannot be detected. Overall, the accuracy of the electron densities from the remote soundings is not as good as the local density measurements. For comparison with Fig. 7, a histogram of the best-fit power-law indices obtained from 102 remote sounding passes is given in Fig. 11. As can be seen the average power-law index, $\langle\gamma\rangle$ = 1.23, is somewhat less than $\gamma$ = 5/3 index characteristic of the Kolmogorov spectrum. This shift is believed to be due to the flattening of the spectrum caused by the quantizing noise at high frequencies. The power law index approaches closer to $\gamma$ = 5/3 if we exclude the high frequency part of the spectrum.

## 5. Altitude dependence

Comparisons of the density fluctuation spectrums in Fig. 10 with those in Fig. 5 show that the spectrums obtained from the remote density measurements at low altitudes are substantially more intense than the spectrums obtained from the local measurements at higher altitudes. This would seem to imply that the source of the fluctuations is at low altitudes. To investigate this altitude dependence, we have sorted all of the available local density measurements into 15 km altitude bins and computed the standard deviation, $\Delta n_e$, of the electron density in each altitude bin. The standard deviation, which is a measure of the deviation from the mean, is assumed to be proportional to the average amplitude of the density fluctuations. The data have also been

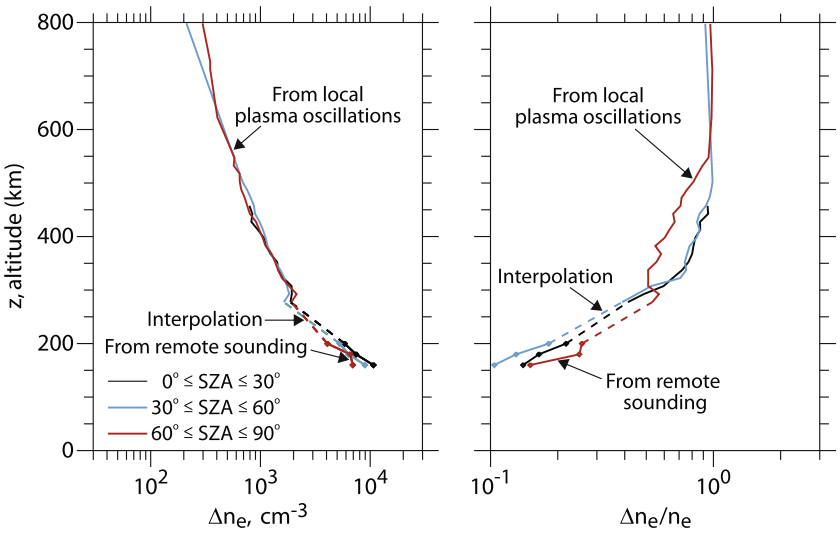


**Fig. 12.** The left-hand panel shows a plot of the standard deviation, $\Delta n_e$, of the electron density as a function of altitude, and the right-hand panel shows the standard deviation divided by the average density in each altitude bin, $\Delta n_e/n_e$, as a function of altitude. The data above 275 km are all from local measurements, and the data below 275 km are all from remote sounding measurements. The dashed lines are interpolations between the two types of measurements.

sorted into three SZA ranges, $0° \leqslant \text{SZA} \leqslant 30°$, $30° \leqslant \text{SZA} \leqslant 60°$, $60° \leqslant \text{SZA} \leqslant 90°$. The results are shown in Fig. 12. The panel on the left shows the standard deviation, $\Delta n_e$, in each altitude bin, and the panel on the right shows the standard deviation in each altitude bin divided by the mean density in that bin, $\Delta n_e/n_e$. The local density measurements are marked "from local plasma oscillations" and the remote density measurements are marked "from remote sounding."

As can be seen in Fig. 12 the standard deviation, $\Delta n_e$, clearly increases systematically with decreasing altitude. The altitude variations are remarkably consistent in all three SZA ranges, indicating very little dependence on solar zenith angle. In contrast, the fractional standard deviation, $\Delta n_e/n_e$, decreases with decreasing altitude. The reversal in the slope of these two plots is due to the fact that the mean electron density increases with decreasing altitude much faster than the standard deviation. The increase in the standard deviation with decreasing altitude would seem to support the idea that the fluctuations originate from a source at low altitudes. On the other hand, the increase in the fractional standard deviation with increasing altitude would seem to support the idea of a source at high altitude. Unfortunately, we have no direct experimental way of determining the direction of vertical energy transport associated with these fluctuations, so the implication regarding the source location must rely on physical interpretation which is discussed in the next section.

## 6. Discussion

We have shown that the upper ionosphere of Mars is dominated by a persistent level of very large density fluctuations. The density fluctuations are so large that a clearly defined boundary between the ionosphere and the solar wind, such as the ionopause at Venus (Brace et al. 1983), is rarely observed. The power spectrums of both the density and magnetic field fluctuations are consistent with the Kolmogorov spectrum expected for isotropic three-dimensional fluid turbulence. The close similarity of the density and magnetic field spectrums suggests that the turbulence may consist of compressional Alfvén waves or mirror-mode waves, both of which are known to have correlated density and magnetic field fluctuations. Although the waveforms of the density and magnetic field fluctuations occasionally show a one-to-one correlation, in general the correlation between the two waveforms is poor. The poor correlation suggests that the magnetic field fluctuations may also include a significant level of shear Alfvén waves, which have magnetic field fluctuations but no density fluctuations, or some other more complex magnetic field structures, such as flux ropes. Unfortunately, since we cannot measure the direction of the magnetic field, our ability to analyze the relationship between the density and magnetic field fluctuations is quite limited. The remote sounding measurements show that the density fluctuations have a good two-point correlation if the altitude separation is small, 20 km or less. However, the correlation decreases rapidly with increasing altitude separation, to the point that no correlation is obvious between the density fluctuations in the remote and local density measurements, which are usually separated by altitudes of 100 km or more. This decline in the correlation with increasing altitude separation indicates that the characteristic spatial correlation scale of the turbulence is probably not more than 20 to 50 km. A statistical study of the amplitude of the fluctuations shows that the standard deviation of the fluctuations, $\Delta n_e$, increases with decreasing altitude. However, the fractional standard deviation of the fluctuations, $\Delta n_e/n_e$, has the opposite dependence and decreases with decreasing altitude.

The primary interpretational questions that arise from this study have to do with the source of the density fluctuations and their mode of propagation. Four possible sources have been considered. These are illustrated in Fig. 13 and can be categorized into two types: first, upward propagating disturbances originating from near the planet, and second, downward propagating disturbances that originate from the solar wind. Sources in the first category consist of (1) propagating disturbances caused by atmospheric waves excited by topographical features on Mars (Hinson et al. 2001; Wang and Nielsen 2004), and (2) propagating disturbances produced by the interaction of the ionosphere with crustal magnetic fields (Ness et al. 2000; Krymskii et al. 2003, 2004; Eastwood et al. 2008). Sources in the second category consist of (1) solar wind plasma and magnetic field disturbances incident on the dayside ionosphere (Wang and Nielsen 2003), (2) waves generated by the mirror-mode instability in the magnetosheath (Volwerk et al., 2008), and (3) waves originating from the Kelvin–Helmholtz instability caused by the velocity shear between the rapidly flowing magnetosheath and the nearly stationary ionosphere (Penz et al. 2004). Although the amplitude of the density fluctuations de-

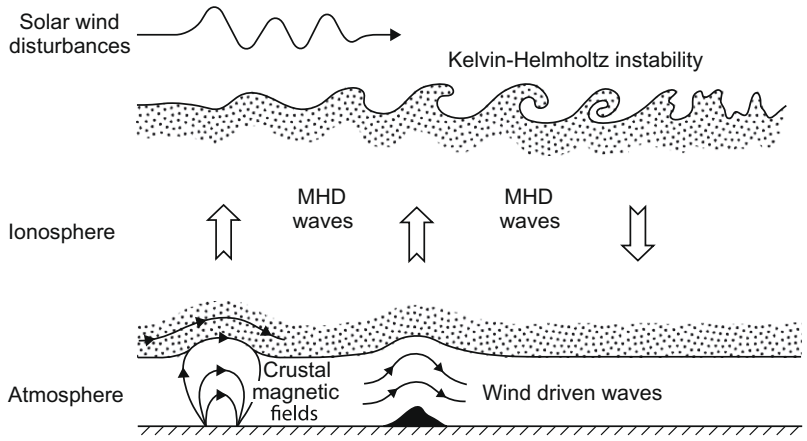


**Fig. 13.** Five possible sources are known for the large density fluctuations observed in the martian ionosphere. At low altitudes possible sources consist of (1) atmospheric waves driven by wind flowing over surface features such as mountains, and (2) ionospheric waves driven by interactions with crustal magnetic fields. At high altitudes possible sources consist of (1) waves driven by solar wind plasma and magnetic field disturbances incident on the ionosphere, (2) waves driven by the mirror-mode instability in the magnetosheath, and (3) waves driven by the Kelvin–Helmholtz instability caused by the velocity shear between the magnetosheath and the ionosphere.

creases with increasing altitude, suggesting a source near the planet, our studies do not generally support a planetary source as the origin of the persistent level of fluctuations that is commonly observed. Although there is evidence of a crustal magnetic field source in isolated cases, the low-altitude remote sounding measurements generally show a statistically poor correlation between the density fluctuations and either topographical features or crustal magnetic fields. In particular, large density fluctuations are commonly observed over the northern regions of Mars where the surface terrain is relatively smooth and the crustal magnetic fields are generally very small.

If the general level of density fluctuations does not originate from a low altitude source, then we must consider the solar wind or magnetosheath as the likely source. Three sources of fluctuation are known to occur in this region. First, Wang and Nielsen (2002, 2003) have proposed that solar wind plasma and magnetic disturbances incident on the dayside ionosphere could produce large density fluctuations that propagate downward into the ionosphere. Second, at Earth and Venus it is known that the mirror-mode instability causes large amplitude density and magnetic field fluctuation to grow in the magnetosheath downstream of the bow shock (Tsurutani et al., 1982; Volwerk et al., 2008). Third, Penz et al. (2004), have proposed that velocity shear between the solar wind and the ionosphere could produce large density fluctuations in the ionosphere via the Kelvin–Helmholtz instability. Of these three possibilities, we believe that the most likely source is either the Kelvin–Helmholtz instability or the mirror-mode instability. However, we cannot rule out solar wind disturbances as a possible contributing source. Kopf et al., (2008) have observed transient layers in the upper ionosphere on the dayside of Mars at solar zenith angels less than about 60° that could very well be caused by such solar wind disturbance. Unfortunately, the absence of a suitable upstream monitor in the solar wind makes it very difficult to evaluate solar wind disturbances as a source. The primary evidence supporting the Kelvin–Helmholtz instability as the source is given by the altitude dependence of the fractional density fluctuations shown in Fig. 12. As can be seen, the amplitude of the fractional density fluctuations increases rapidly with increasing altitude, from relatively small values of $\Delta n_e/n_e \sim 0.1$ around 160 km, to near one, $\Delta n_e/n_e \sim 1$, at altitudes of 400 km and above. The very large values of $\Delta n_e/n_e \sim 1$ at about 400 km indicate that the turbulence is completely saturated, i.e., the density fluctuations have reached their largest possible amplitude, i.e., $\Delta n_e \sim n_e$. We believe that it is significant that the fluctuations reach saturation at an altitude of about 400 km, which is the nominal altitude expected for the boundary between the dayside ionosphere and the solar wind (Trotignon et al. 2006; Dubinin et al. 2006).

Further evidence that the density fluctuations are due to the Kelvin–Helmholtz instability is given by the density waveforms in Fig. 3, which tends to show transitions between two density states that are correlated with solar wind incursions into the ionosphere. Such transitions, which are commonly observed in the altitude range around 400 km, strongly suggest that the spacecraft is passing through an irregular sine wave-like boundary between the relatively dense ionospheric plasma and the more tenuous magnetosheath plasma. This is exactly what would be expected in the region where the Kelvin–Helmholtz instability causes mixing of the two plasmas. Although the above arguments favor the Kelvin–Helmholtz instability, there are still unresolved problems. Since the Kelvin–Helmholtz instability is driven by the horizontal velocity component of the solar wind, the instability is not expected to be excited in the vicinity of the sub-solar point, where the horizontal component of the solar wind velocity is small. Since large density fluctuations are observed near the sub-solar point, this may indicate that fluctuations in the solar wind pressure or the mirror-mode instability in the magnetosheath may play the dominant role in this region.

If the main source of the density fluctuations is near the magnetosheath-ionosphere boundary, it remains to be explained why the standard deviation of the fluctuations increases with decreasing altitude, as shown in the left-hand panel of Fig. 12. A solar wind/magnetosheath source implies that the energy flow in the turbulent fluctuations must be directed downwards, so we must consider the mechanism by which the fluctuations are transmitted. Although the wave energy may be transported horizontally due to a horizontal component of the ionospheric motion, for our purposes we concentrate only on the vertical component of the wave motion. If the energy is propagated downward from the magnetosheath region as a compressional Alfvén wave, which seems to be the most likely mode of propagation, then there are good reasons to think that amplitude of the fluctuations would increase with decreasing altitude. The explanation is similar to the increase in the amplitude of an ocean wave propagating into a shallow sloping beach. According to the WKB (Wentzel–Kramer–Brillouin) theory for wave propagation through a slowly varying medium (Budden 1961), if the energy flux is conserved, then the product of the wave amplitude squared times the downward component of the group velocity must be constant, i.e., $A^2 v_g$ = constant. This relation im-

plies that the amplitude should be proportional to the inverse square root of the group velocity, $A \sim 1/\sqrt{v_g}$. For an ocean wave propagating into a shallow beach the group velocity is proportional to the square root of the depth, $v_g \sim \sqrt{h}$, so as the wave propagates into the beach the amplitude increases as the depth decreases (Fetter and Walecka, 1980). For a compressional Alfvén wave the group velocity is given by $v_g = B_0/\sqrt{\mu_0 \rho_{m0}}$, where $B_0$ is the zero-order magnetic field and $\rho_{m0}$ is the zero-order mass density (Gurnett and Bhattacharjee, 2005). This equation, together with the $A^2 v_g$ = constant condition, implies that the wave amplitude should vary as $(\rho_{m0})^{1/4}/B_0^{1/2}$. Because the mass density in the ionosphere, $\rho_{m0}$, increases exponentially with decreasing altitude and varies much more rapidly than the magnetic field strength $B_0$, the amplitude of a downward propagating Alfvén wave should increase exponentially with decreasing altitude. Preliminary estimates, taking into account the scale height of the ionosphere (Morgan et al., 2008) and the relatively weak altitude dependence of the solar wind induced magnetic field (Brain, 2007), show that the exponential amplitude variation implied by the above model has the qualitatively correct trend to explain the altitude shown in Fig. 12. However, the exponential increase is not sufficiently rapid, by about a factor of two in the logarithmic slope, $d(\log n_e)/dz$, to explain the observed altitude dependence. This discrepancy possibly indicates that that there may be a significant upward propagating contribution from a low altitude source, or that some other vertical energy transport mechanism is involved in downward propagation. Whether and under what conditions the Kelvin–Helmholtz instability, the mirror-mode instability, and/or pressure disturbances in the solar wind are responsible for the complex density and magnetic field fluctuations observed in the martian ionosphere will require further study.

## Acknowledgments

This research was supported by NASA through contract 1224107 from the Jet Propulsion Laboratory.

## References

Acuña, M.H., and 19 colleagues, 1998. Magnetic field and plasma observations at Mars: Initial results of the Mars Global Surveyor mission. S cience 279, 1676–1680.

Acuña, M.H., and 12 colleagues, 1999. Global distribution of crustal magnetization discovered by the Mars Global Surveyor MAG/ER experiment. S cience 284, 790–793.

Barabash, S., and 47 colleagues, 2004. ASPERA-3: Analyser of space plasmas and energetic ions for Mars Express. In: Wilson, A. (Ed.), SDF SFSF, sPRINGER, bERLIN, pp. 121–139.

Brace, L.H., Taylor Jr., H.A., Gombosi, T.I., Kliore, A.J., Knudsen, W.C., Nagy, A.F., 1983. The ionosphere of Venus: Observations and their interpretation. In: Hunten, D.M., Colin, L., Donahue, T.M., Moroz, V.I. (Eds.), Venus. Univ. of Arizona Press, Tucson, AZ, pp. 779–840.

Brain, D.A., Bagenal, F., Acuña, M.H., Connerney, J.E.P., 2003. Martian magnetic morphology: Contribution from the solar wind and crust. J. Geophys. Res. 108 (A12), 1424. doi:10.1029/2002JA009482.

Brain, D.A., Mitchell, D.L., Halekas, J.S., 2006. The magnetic field draping direction at Mars from April 1999 through August 2004. Icarus 182, 464–473.

Brain, D.A., 2007. Mars Global Surveyor measurements of the martian solar wind interaction. Space Sci. Rev. 126, 77–112. 10.107/s11214-006-9122-x.

Budden, K.G., 1961. Radio Waves In the Ionosphere: The Mathematical Theory of the Reflection of Radio Waves From Stratified Ionized Layers. Cambridge Univ. Press, London.

Cain, J.C., Ferguson, B.B., Mozzoni, D., 2003. An $n = 90$ internal potential function of the martian crustal magnetic field. J. Geophys. Res. 108 (E2), 5008. doi:10.1029/2000JE001487.

Chicarro, A., Martin, P., Traunter, R., 2004. The Mars Express mission: An overview. In: Wilson, A. (Ed.), Mars Express: A European Mission to the Red Planet, SP-1240, European Space Agency Publication Division. Noordwijk, Netherlands, pp. 3–16.

Connerney, J.E.P., Acuña, M.H., Ness, N.F., Kletetschka, G., Mitchell, D.L., Lin, R.P., Rème, H., 2005. Tectonic implications of Mars crustal magnetism. Proc. Nat. Acad. Sci. 102, 14970–14975.

Dubinin, E., Fränz, M., Woch, J., Roussos, E., Barabash, S., Lundin, R., Winningham, J.D., Frahm, R.A., Acuña, M., 2006. Plasma morphology at Mars. ASPERA-3 observations. Space Sci. Rev. 126, 209–238. doi:10.1007/s11214-006-9039-4.

Duru, F., Gurnett, D.A., Averkamp, T.F., Kirchner, D.L., Huff, R.L., Persoon, A.M., Plaut, J.J., Picardi, G., 2006. Magnetically controlled structures in the ionosphere of Mars. J. Geophys. Res. 111, A12204. doi:10.1029/2006JA011975.

Duru, F., Gurnett, D.A., Morgan, D.D., Modolo, R., Nagy, A.F., Najib, D., 2008. Electron densities in the upper ionosphere of Mars from the excitation of electron plasma oscillations. J. Geophys. Res. 113, A07302. doi:10.1029/2008JA013073.

Eastwood, J.P., Brain, D.A., Halekas, J.S., Drake, J.F., Phan, T.D., Øieroset, M., Mitchell, D.L., Lin, R.P., Acuña, M., 2008. Evidence for collisionless magnetic reconnection at Mars. Geophys. Res. Lett. 35, L02106. doi:10.1029/2007GL032289.

Fetter, A.L., Walecka, J.D., 1980. Theoretical Mechanics of Particles and Continua. McGraw-Hill, New York. p. 372.

Fjeldbo, G., Fjeldbo, W.C., Eshleman, V.R., 1966. Models for the atmosphere of Mars based on the Mariner 4 occultation experiment. J. Geophys. Res. 71, 2307–2316.

Gurnett, D.A., Bhattacharjee, A., 2005. Introduction to Plasma Physics with Space and Laboratory Applications. Cambridge Univ. Press, Cambridge. p. 91.

Gurnett, D.A., and 10 colleagues, 2005. Radar soundings of the ionosphere of Mars. S cience 310, 1929–1933.

Gurnett, D.A., and 12 colleagues, 2008. An overview of radar soundings of the martian ionosphere from the Mars Express spacecraft. Adv. Space Research 41 (9), 1335–1346. doi: 10.1016/j.asr.2007.01.062.

Hinson, D.P., Tyler, G.L., Hollingsworth, J.L., Wilson, R.J., 2001. Radio occultation measurements of forced atmospheric waves on Mars. J. Geophys. Res. 106, 1463–1480.

Kopf, A.J., Gurnett, D.A., Morgan, D.D., Kirchner, D.L., 2008. Transient layer in the topside ionosphere of Mars. Geophys. Res. Lett. 35, L17102. doi:10.1029/2008GL034948.

Kliore, A.J. 1992. Radio occultation observations of the ionospheres of Mar and Venus. In: Luhmann, J.G., Tatrallyay, M., Pepin, R. (Eds.), Venus and Mars, Ionospheres, and Solar Wind Interactions. In: Geophysics Monograph Series, vol. 66. Am. Geophys. Union, Washington, DC, pp. 265–276.

Kolmogorov, A.N., 1941. The local structure of turbulence in incompressible viscous fluid for very large Reynolds numbers. Dokl. Akad. Nauk SSSR 30, 299–303.

Krymskii, A.M., Breus, T.K., Ness, N.F., Hinson, D.P., Bojkov, D.I., 2003. Effect of crustal magnetic fields on the near terminator ionosphere at Mars: Comparison of in situ magnetic field measurements with the data of radio science experiments on board Mars Global Surveyor. J. Geophys. Rev. 108 (A12), 1431. doi:10.1029/2002JA009662.

Krymskii, A.M., Ness, N.F., Crider, D.H., Breus, T.K., Acuña, M.H., Hinson, D.P., 2004. Solar wind interaction with the ionosphere/atmosphere and crustal magnetic fields at Mars: Mars Global Surveyor magnetometer/electron reflectometer, radio science, and accelerometer data. J. Geophys. Res. 109, A11306. 1029/2004JA010420.

Luhmann, J.G., Brace, L.H., 1991. Near-Mars space. Rev. Geophys. 29, 121–140.

Mendillo, M., Pi, X., Smith, S., Martinis, C., Wilson, J., Hinson, D., 2004. Ionospheric effects upon a satellite navigation system at Mars. Radio Sci. 39, RS2028. doi:10.1029/2003RS002933.

Morgan, D.D., Gurnett, D.A., Kirchner, D.L., Fox, J.L., Nielsen, E., Plaut, J.J., 2008. Variation of the martian ionospheric electron density from Mars Express radar soundings. J. Geophys. Res. 113, A09303. doi:10.1029/2008JA013313.

Nielsen, E., Zhou, H., Gurnett, D.A., Kirchner, D.L., Morgan, D.D., Huff, R.L., Orosei, R., Safaeinili, A., Plaut, J.J., Picardi, G., 2006. Observations of vertical reflections from the topside martian ionosphere. Space Sci. Rev. 126, No. 1–4. doi: 10.1007/s11214-006-9113-y.

Nielsen, E., Wang, X.-D., Gurnett, D.A., Kirchner, D.L., Huff, R.L., Orosei, R., Safaeinili, A., Plaut, J.J., Picardi, G., 2007. Vertical sheets of dense plasma in the topside martian ionosphere. J. Geophys. Res. 112, E02003. 1029/2006JE002723.

Ness, N.F., Acuña, M.H., Connerney, J.E.P., Kliore, A.J., Breus, T.K., Krymskii, A.M., Cloutier, P., Bauer, S.J., 2000. Effects of magnetic anomalies discovered at Mars on the structure of the martian ionosphere and solar wind interaction as follows from radio occultation experiments. J. Geophys. Res. 105, 15,991–16,004.

Pätzold, M., Tellmann, S., Häusler, B., Hinson, D., Schaa, R., Tyler, G.L., 2005. A sporadic third layer in the ionosphere of Mars. Science 310, 837–839.

Penz, T., and 10 colleagues, 2004. Ion loss on Mars caused by the Kelvin-Helmholtz instability. Planet. Space Sci. 52, 1157–1167.

Picardi, G., and 12 colleagues, 2004. MARSIS: Mars advanced radar for subsurface and ionosphere sounding. In: Wilson, A. (Ed.), sdfd ffsf, Springer, Berlin. pp. 51–69.

Russell, C.T., Elphic, R.C., 1979. Observations of flux ropes of the Venus ionosphere. Nature 279, 616–618.

Savich, N.A., Samovol, V.A., 1976. The nighttime ionosphere of Mars from Mars-4 and Mars-5 dual-frequency radio occultation measurements. Space Res. 16, 1009–1010.

Terada, N., Machida, S., Shinagawa, H., 2002. Global hybrid simulation of the Kelvin–Helmholtz instability at the Venus ionopause. J. Geophys. Res. 107 (A12), 1471. doi:10.1029/2001JA009224.

Terada, N., Shinagawa, H., Machida, S., 2004. Global hybrid model of the solar wind interaction with the Venus ionosphere: Ion escape processes. Adv. Space Res. 33, 162–166. doi:10.1016/j.asr.2003.05.011.

Trotignon, J.G., Mazelle, C., Bertucci, C., Acuña, M.H., 2006. Martian shock and magnetic pile-up boundary positions and shapes determined from the Phobos 2 and Mars Global Surveyor data sets. Planet. Space Sci. 54, 357–369.

Tsurutani, B.T., Smith, E.J., Anderson, R.R., Ogilvie, K.W., Scudder, J.D., Baker, D.N., Bame, S.J., 1982. Lion roars and nonoscillatory drift mirror mode waves in the magnetosheath. J. Geophys. Res. 87, 6060–6072.

Vignes, D., Acuna, M.H., Connerney, J.E.P., Crider, D.H., Reme, H., Mazelle, C., 2004. Magnetic flux ropes in the martian atmosphere: Global characteristics. Space Sci. Rev. 111, 223–231.

Volwerk, M., Zhang, T.L., Delva, M., Vörös, Z., Baumjohann, W., Glassmeier, K.-H., 2008. First identification of mirror mode waves in Venus' magnetosheath? Geophys. Res. Lett. 35, L12204. doi:10.1029/2008GL033621.

Wang, J.-S., Nielsen, E. 2002. Dispersion relation and numerical simulation of hydrodynamic waves in Mars' topside ionosphere. Paper presented at the 27th General Assembly of the European Geophysical Society, Nice, France.

Wang, J.-S., Nielsen, E., 2003. Wavelike structures in the martian topside ionosphere observed by Mars Global Surveyor. J. Geophys. Res. 108 (E7), 5078. doi:10.1029/2003JE002078.

Wang, J.-S., Nielsen, E., 2004. Evidence for topological effects on the martian ionosphere. Planet. Space Sci. 52, 881–886. doi:10.1016/j.pss.2004.01.008.

Whittaker, E.T., Watson, G.N., 1927. Modern Analysis, fourth ed. Cambridge Univ. Press, New York. p. 229.

Withers, P., Mendillo, M., 2005. Response of peak electron densities in the martian ionosphere to day-to-day changes in solar flux. Planet. Space Sci. 53, 1401–1418. doi:10.1016/j.pss.2005.07.010.

Zhang, M.H.G., Luhmann, J.G., Kliore, A.J., 1990a. A post Pioneer Venus reassessment of the martian dayside ionosphere as observed by radar occultation methods. J. Geophys. Res. 95, 14,829–14,839.

Zhang, M.G.H., Luhmann, J.G., Kliore, A.J., 1990b. An observational study of the nightside ionosphere of Mars and Venus with radio occultation methods. J. Geophys. Res. 95, 17095–17102.